to account for the buffer-independent reactions.

Conclusion

In view of the serious discrepancies noted above, it is apparent that Breslow's proposed mechanism and postulated reactions of the common intermediate as in Schemes I or II are not supported by the measured[3,4] functional dependences of the rates of cleavage and isomerization. Modifications to the mechanism, such as the addition of buffer-dependent terms to the reaction of the intermediate that leads to isomerization or reversing the role of the two components of the buffer, but keeping the requirement of a common intermediate, also yield rate laws incompatible with the reported functional dependences. Since the key claims in BH and AB are based on the purported agreement between rate measurements and proposed mechanism, it is evident that several of Breslow's mechanistic inferences can no longer be taken as proven. One of the claims in AB is that two mechanisms that bear a mirror image relationship are indistinguishable on the basis of the kinetic measurements of cleavage only, but that the ambiguity was resolved by considering the kinetics of isomerization. With the revelation that the proposed mechanism is incompatible with the reported rates, the kinetic ambiguity remains unresolved. The case for questioning BH is even more compelling because here the whole study revolves around the flawed[22] demonstration of a common intermediate.

In the foregoing analyses of the kinetic measurements and of the implications of the proposed mechanism and kinetic model, the reported rate constants were taken at face value. However, it must be noted that the studies were carried out at variable ionic strength[23] and pH[24] and therefore the reported rate measurements are of limited value in arriving at detailed mechanistic conclusions.[25] Under these circumstances, although the proposed mechanism and the claim of a common intermediate are not sustained by the kinetic data, some of the postulated reactions in Schemes I or II may be operative.

Acknowledgment. Helpful discussions with several of my colleagues are gratefully acknowledged. The author is grateful to Professor F. M. Menger for encouragement and for a preprint of ref 5.

(22) In principle, detailed kinetic and stoichiometric studies are helpful in demonstrating the occurrence of intermediates along reaction pathways. In this context, we note that Breslow's claim[4] of an "unusual kinetic tool" is a minor variation on the well-known common ion retardation and chemical competition methodologies: Ingold, C. K. *Structure and Mechanism in Organic Chemistry*; Cornell University Press: New York, 1953.

(23) Since the pK_a of ImH^+ varies with ionic strength (the values are 7.01, 7.18, 7.31, and 7.90 at 25 °C and ionic strength 0.1, 0.5, 1.0, and 3.0: Smith, R. M.; Martell, A. E. *Critical Stability Constants*; Plenum: New York, 1989; Vol. 5), even solutions with the same $[ImH^+]/[Im]$ ratio will differ slightly in pH.

(24) Nearly half the measurements were carried out with only one of the two buffer components added and therefore at variable pH. For example, the calculated values of pH for 0.10 and 1.0 M solutions of imidazole are 10.0 and 10.7, respectively.

(25) Specifically, we note that the bulk of the experiments which exhibit a decrease in rate of isomerization with increasing buffer concentration (and thus negative corrected rate constants) were carried out at 0 state of protonation (only imidazole, no imidazolium added). Under these circumstances, an increase in imidazole is accompanied by an increase in pH.[24] Since there is evidence that the rate of the buffer-independent isomerization decreases with increasing pH (the intercepts at 0 buffer concentration in Figures 5 and 6 of AB increase with a decrease in pH), the reported decrease in rate with increasing imidazole concentration may simply be a manifestation of the decrease in the rate of the buffer-independent contribution and may bear no relationship to the mechanism of the buffer-catalyzed pathways.

Computational Study of Jahn–Teller Type Distortions in Radical Cations of Methyl-Substituted Cyclopropanes

Karsten Krogh-Jespersen* and Heinz D. Roth*

Contribution from the Department of Chemistry, Rutgers, The State University of New Jersey, New Brunswick, New Jersey 08903. *Received April 22, 1992*

Abstract: We have studied Jahn–Teller (JT) type distortions in a series of methyl-substituted cyclopropane cations with ab initio molecular orbital techniques. Two sets of cyclopropane cation structures are considered for the parent (**1a**) and the 1-methyl-substituted (**1b**), 1,1-dimethyl-substituted (**1c**), 2,3-dimethyl-substituted (**1d** (trans), **1e** (cis)), and 2,2,3,3-tetramethyl-substituted (**1f**) species. These structures reflect the first-order JT distortions occurring in the parent cation (**1a**) from a doubly degenerate $^2E'$ (D_{3h} symmetry) ground state to nondegenerate states of $^2A_1$ and $^2B_2$ symmetry (C_{2v} point group). States of the "$^2A_1$ type" possess one long and two short ring C–C bonds, are always structural minima on their respective potential energy surfaces, and represent the minimum energy structures for **1a**, **1d**, **1e**, and **1f**. The "$^2B_2$-type" states are structurally characterized by two long and one short ring C–C bonds and are always transition states, although they are the preferred first-order JT type distorted structures for both 1-methylated cations (**1b,c**). Unsymmetrical (scalene) triangular structures actually represent the absolute minima for **1b** and **1c**. These structures may be viewed as distorted from the "$^2B_2$-type" geometries via a second-order JT type mechanism or, alternatively, as "$^2A_1$-type" with the substituents at the "wrong" carbon atom. The predicted fine-tuning of cation state preference and substantial differences in spin density distributions should be verifiable by spectroscopic means (ESR). The qualitative charge density distributions might be probed by chemical means (nucleophilic capture); an unequivocal interpretation is questionable, however.

Radical cations of cyclopropane (**1a**) and derivatives have attracted considerable attention for over one decade. Molecular orbital calculations suggest that the vertical ionization of cyclopropane occurs from a degenerate pair of in-plane e′ orbitals (**2**, **3**); first-order Jahn–Teller (JT) distortion of the resulting doubly degenerate $^2E'$ state leads to two nondegenerate electronic states, $^2A_1$ and $^2B_2$ (C_{2v} symmetry).[1-7] The $^2A_1$ component (orbital **2** singly occupied) relaxes to an equilibrium structure with one lengthened C–C bond, which is accepted as the lowest energy

(1) Haselbach, E. *Chem. Phys. Lett.* **1970**, *7*, 428.
(2) Rowland, C. G. *Chem. Phys. Lett.* **1971**, *9*, 169.
(3) Collins, J. R.; Gallup, G. A. *J. Am. Chem. Soc.* **1982**, *104*, 1530.
(4) Bouma, W. J.; Poppinger, D.; Radom, L. *Isr. J. Chem.* **1983**, *23*, 21.

0002-7863/92/1514-8388$03.00/0

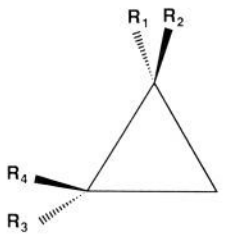

1a: $R_1, R_2, R_3, R_4 = H$
1b: $R_1 = CH_3$; $R_2, R_3, R_4 = H$
1c: $R_1, R_2 = CH_3$; $R_3, R_4 = H$
1d: $R_1, R_4 = CH_3$; $R_2, R_3 = H$
1e: $R_1, R_3 = CH_3$; $R_2, R_4 = H$
1f: $R_1, R_2, R_3, R_4 = CH_3$

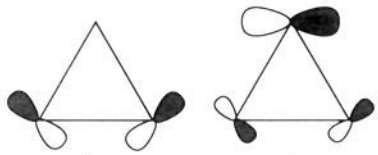

2 3

species for many cyclopropane radical cations. These assignments are compatible with a number of experimental findings, including low-temperature ESR spectra of the parent ion;[8] CIDNP[9] or ESR spectra[10] for di-, tri-, and tetrasubstituted derivatives; and various electron-transfer-induced ring-opening reactions.[10–15] Most recently, the opening of $^2A_1$ radical cations to trimethylene species was deduced from low-temperature ESR studies,[10] but this assignment was questioned on the basis of ab initio calculations[5,6] and other arguments.[5,16]

Elementary considerations suggest that substitution at a single carbon will preferentially stabilize the $^2B_2$ component (orbital **3** singly occupied) and generate a structure in which two C–C bonds are lengthened and one is shortened. In this paper, we call particular attention to this potentially accessible $^2B_2$ radical cation state and explore the possible existence of such radical cations. Their spin and charge density distributions and, hence, their chemistry may differ substantially from those determined for cyclopropane cations studied previously.

Computational Details

Ab initio calculations[17] were carried out for the parent (**1a**) and for monomethyl-substituted (**1b**), dimethyl-substituted (**1c–e**), and tetramethyl-substituted (**1f**) cyclopropane cations with the GAUSSIAN 88 and GAUSSIAN 90 series of electronic structure programs.[18] Molecular structures were optimized at the unrestricted Hartree–Fock (UHF) level with the 6-31G* basis set (UHF/6-31G*//UHF/6-31G*); the optimized C–C bond lengths are listed in Table I. Full normal coordinate analysis using analytical expressions for the second derivatives of the energy was made to characterize the located stationary points as minima or transition states, and the computed vibrational frequencies also produced zero-point energies (ZPE, Table II). Total energies including electron correlation contributions were obtained at the optimized geometries using Møller–Plesset perturbation theory, mostly through fourth-order (UMP4(SDTQ)/6-31G*//UHF/6-31G*), Table II. We have also tabulated the spin projected results (PMP4(SDTQ)/6-31G*//UHF/6-31G*), and we combined these total energies with the ZPE corrections to form the relative energies (ΔE, Table II). These values will be quoted in the text unless otherwise noted. Selected calculations, to be discussed individually, were made with a larger basis set (6-311G*), included correlation in the geometry optimization (UMP2/6-31G*), or used configuration interaction including all single and double excitations (CISD) as the method for assessing the energetic effects of electron correlation. For the correlated wave functions, the normal mode analyses were made numerically using finite differences of analytically computed first derivatives to approximate the second derivatives of the energy. Wavefunction analyses for charge and spin density distributions were performed using the conventional Mulliken partitioning scheme.[17]

Results and Discussion

Geometries and Energetics. Although all the methylated species (**1b–f**) inherently possess considerably lower molecular symmetries than the parent cation (**1a**), they are expected to, and actually do, undergo first-order JT type distortions to isosceles triangular structures in full accordance with their parentage and the orbital compositions of **2** and **3**. The two relevant electronic states transform according to different irreducible representations in each of the point groups represented by **1a–f**; specifically, the actual symmetries are $^2A_1$, $^2B_2$ (**1a,c,f**; C_{2v}); $^2A'$, $^2A''$ (**1b,e**; C_s); and ^2A, ^2B (**1d**; C_2). For convenience, we will label them collectively as "$^2A_1$-type" or "$^2B_2$-type". The "$^2A_1$-type" states generate structures (**4**) that are trimethylene-like and characterized by one very long

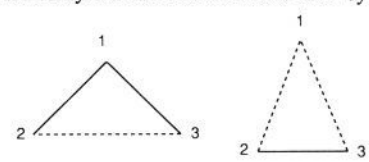

4 5

(1.85–1.95 Å) and two relatively short (~1.48 Å) ring C–C bonds (Table I), the former being indicative of a one-electron, two-center bond. The "$^2B_2$-type" states feature structures (**5**) with one short (~1.40 Å) and two long (~1.68 Å) ring C–C bonds and are usually described as π (or "tight") complexes formed between a methylene cation and an ethene.[4,5,9b] For comparison, the optimized C–C bond length in neutral cyclopropane is 1.497 Å (RHF/6-31G*//RHF/6-31G*).

In agreement with experimental ESR data[8] and previous ab initio studies on **1a** with basis sets of at least split-valence quality,[4,5] we find that the $^2A_1$ state (**4a**) is slightly more stable (2.5 kcal/mol, Table II) than the $^2B_2$ state (**5a**). The stationary point located for the $^2B_2$ state is not a minimum on the potential energy surface, also in agreement with previous computational studies. It has one imaginary frequency for in-plane distortion ($518i$ cm^{-1}, b_2 symmetry) and relaxes upon structural reoptimization in C_s symmetry without an energy barrier to the equilibrium structure representing the $^2A_1$ state. The authors of ref 3, using a minimal STO-3G basis set and limited configuration interaction, found not only a larger and inverted energy separation ($^2B_2$ lower than $^2A_1$ by 6.7 kcal/mol) but also that neither electronic state was a minimum on the potential energy surface; instead, a scalene triangular structure with three substantially different C–C bond lengths (1.698, 1.861, 1.533 Å) was located about 0.7 kcal/mol below the $^2B_2$ state (7.3 kcal/mol below $^2A_1$). Since we do obtain related unsymmetrical structures as minima for the 1-substituted cyclo-

(5) Wayner, D. D. M.; Boyd, R. J.; Arnold, D. R. *Can. J. Chem.* **1985**, *63*, 3283; **1983**, *61*, 2310.
(6) Du, P.; Hrovat, D. A.; Borden, W. T. *J. Am. Chem. Soc.* **1988**, *110*, 3405.
(7) (a) Jahn, H. A.; Teller, E. *Proc. R. Soc. London, A* **1937**, *161*, 220. (b) Pearson, R. G. *J. Am. Chem. Soc.* **1969**, *91*, 4947. Opik, U.; Pryce, M. H. L. *Proc. R. Soc. London, A* **1957**, *238*, 425.
(8) Iwasaki, M.; Toriyama, K.; Nunome, K. *J. Chem. Soc., Chem. Commun.* **1983**, 202.
(9) (a) Roth, H. D.; Schilling, M. L. M. *J. Am. Chem. Soc.* **1980**, *102*, 7956. (b) Roth, H. D.; Schilling, M. L. M. *Can. J. Chem.* **1983**, *61*, 1027. (c) Roth, H. D.; Schilling, M. L. M. *J. Am. Chem. Soc.* **1983**, *105*, 6805. (d) Haddon, R. C.; Roth, H. D. *Croat. Chem. Acta* **1984**, *57*, 1165.
(10) Qin, X. Z.; Snow, L. D.; Williams, F. *J. Am. Chem. Soc.* **1984**, *106*, 7640. Qin, X. Z.; Williams, F. *Tetrahedron* **1986**, *42*, 6301.
(11) Arnold, D. R.; Humphreys, R. W. R. *J. Am. Chem. Soc.* **1979**, *101*, 2743.
(12) Rao, V. R.; Hixson, S. S. *J. Am. Chem. Soc.* **1979**, *101*, 6458.
(13) Mizuno, K.; Ogawa, J.; Kagano, H.; Otsuji, Y. *Chem. Lett.* **1981**, 437. Mizuno, K.; Ogawa, J.; Otsuji, Y. *Chem. Lett.* **1981**, 741.
(14) Gassman, P. G.; Olson, K. D.; Walter, L.; Yamaguchi, R. *J. Am. Chem. Soc.* **1981**, *103*, 4977. Gassman, P. G.; Olson, K. D. *Ibid.* **1982**, *104*, 3740.
(15) Dinnocenzo, J. P.; Todd, W. P.; Simpson, T. R.; Gould, I. R. *J. Am. Chem. Soc.* **1990**, *112*, 2462.
(16) Symons, M. C. R. *Chem. Phys. Lett.* **1985**, *117*, 381.
(17) Hehre et al. present a detailed description of the theoretical methods used in this work. Hehre, W. J.; Radom, L.; Pople, J. A.; Schleyer, P. v. R. *Ab Initio Molecular Orbital Theory*; Wiley Interscience: New York, 1986.
(18) Frisch, M. J.; Head-Gordon, M.; Schlegel, H. B.; Raghavachari, K.; Binkley, J. S.; Gonzalez, C.; Defrees, D. J.; Fox, D. J.; Whiteside, R. A.; Seeger, R.; Melius, C. F.; Baker, J.; Martin, R. L.; Kahn, L. R.; Stewart, J. J. P.; Fluder, E. M.; Topiol, S.; Pople, J. A. *GAUSSIAN 88*; Gaussian, Inc.: Pittsburgh, PA, 1988. Frisch, M. J.; Head-Gordon, M.; Trucks, G. W.; Foresman, J. B.; Schlegel, H. B.; Raghavachari, K.; Robb, M.; Binkley, J. S.; Gonzalez, C.; Defrees, D. J.; Fox, D. J.; Whiteside, R. A.; Seeger, R.; Melius, C. F.; Baker, J.; Martin, R. L.; Kahn, L. R.; Stewart, J. J. P.; Topiol, S.; Pople, J. A. *GAUSSIAN 90*; Gaussian, Inc.: Pittsburgh, PA, 1990.

Table I. Optimized Carbon–Carbon Bond Lengths (Å) for Stationary Points of **1a–f** at the UHF/6-31G* Level (UMP2/6-31G* Optimized Values Are in Parentheses)

species[a]	state[b]	C_1–C_2	C_2–C_3	C_1–C_3	C_1–C_4
4a	$^2A_1$ (M)	1.477 (1.474)	1.875 (1.826)	1.477 (1.474)	
5a	$^2B_2$ (T)	1.682 (1.665)	1.398 (1.410)	1.682 (1.665)	
4b	$^2A'$ (M)	1.481 (1.477)	1.860 (1.807)	1.481 (1.477)	1.524 (1.519)
5b	$^2A''$ (T)	1.676 (1.659)	1.401 (1.415)	1.676 (1.659)	1.487 (1.467)
8b	^2A (T)	1.404 (1.429)	1.727 (1.760)	1.645 (1.557)	1.511 (1.512)
7b	^2A (M)	1.468 (1.462)	1.485 (1.489)	1.917 (1.837)	1.484 (1.467)
4c	$^2A_1$ (M)	1.485	1.848	1.485	1.530
5c	$^2B_2$ (T)	1.676	1.404	1.676	1.496
8c	$^2A'$ (T)	1.417	1.764	1.607	1.523
7c	$^2A'$ (M)	1.468	1.499	1.980	1.492
4d	^2A (M)	1.479	1.888	1.479	1.489
5d	^2B (T)	1.689	1.406	1.689	1.506
4e	$^2A'$ (M)	1.480	1.915	1.480	1.488
5e	$^2A''$ (T)	1.690	1.409	1.690	1.506
4f	$^2A_1$ (M)	1.486	1.984	1.486	1.499
5f	$^2B_2$ (T)	1.699	1.425	1.699	1.519

[a] See structures **4**, **5**, **7**, and **8** for numbering scheme. [b] The nature of the stationary point is indicated in parentheses after the Mulliken terms symbol: M = minimum, T = transition state.

Table II. Ab Initio Total Energies (au), Zero-Point Energies, and Relative Energies (kcal/mol) for Stationary Points of **1a–f** at UHF/6-31G* Optimized Geometries

species[a]	state[b]	UHF/6-31G*	UMP4/6-31G*	PMP4/6-31G*	ZPE[c]	ΔE[d]
4a	$^2A_1$ (M)	−116.749 20	−117.146 66	−117.148 80	52.7 (0)	0.0
5a	$^2B_2$ (T)	−116.742 56	−117.143 55	−117.144 25	52.3 (1)	2.5
4b	$^2A'$ (M)	−155.792 20	−156.337 52	−156.339 79	71.5 (0)	6.8
5b	$^2A''$ (T)	−155.794 62	−156.346 64	−156.347 34	71.5 (1)	2.1
8b	^2A (T)	−155.788 29	−156.337 10	−156.337 98	71.1 (1)	7.5
7b	^2A (M)	−155.802 07	−156.348 86	−156.350 81	71.6 (0)	0.0
4c	$^2A_1$ (M)	−194.833 03	−195.528 19	−195.530 57	90.5 (0)	12.9
5c	$^2B_2$ (T)	−194.843 15	−195.546 36	−195.547 05	90.6 (1)	2.6
8c	$^2A'$ (T)	−194.831 41	−195.529 08	−195.530 37	89.8 (1)	12.3
7c	$^2A'$ (M)	−194.853 54	−195.548 63	−195.550 43	90.1 (0)	0.0
4d	^2A (M)	−194.853 01	−195.550 01	−195.551 92	90.7 (0)	0.0
5d	^2B (T)	−194.838 70	−195.536 37	−195.537 17	90.0 (1)	8.6
4e	$^2A'$ (M)	−194.851 72	−195.548 76	−195.550 66	90.8 (0)	0.0
5e	$^2A''$ (T)	−194.836 48	−195.534 52	−195.535 32	90.0 (1)	8.8
4f	$^2A_1$ (M)	−272.942 56	−273.828 49[e]		128.1 (0)[f]	0.0
5f	$^2B_2$ (T)	−272.916 64	−273.805 00[e]		127.0 (1)[f]	13.6

[a] See structures **4**, **5**, **7**, and **8** for numbering scheme. [b] The nature of the stationary point is indicated in parentheses after the Mulliken term symbol: M = minimum, T = transition state. [c] Number of imaginary frequencies is indicated in parentheses. Imaginary frequencies are not included in ZPE calculations. [d] Relative energy obtained by combining differential PMP4(SDTQ)/6-31G*//UHF/6-31G* and differential ZPE energies. [e] Computed at the UMP2/6-31G*//UHF/6-31G* level. [f] Computed at the UHF/3-21G//UHF/3-21G level.

propane cations **1b** and **1c** (see below), we decided to carry the calculations on the simpler parent system (**1a**) further.

After configuration interaction with all single and double substitutions included (CISD/6-31G*//UHF/6-31G* + ΔZPE), the $^2B_2$–$^2A_1$ energy difference is 2.2 kcal/mol in favor of $^2A_1$.[19a] Geometry optimization at the second-order Møller–Plesset level (UMP2/6-31G*) shortens the very long C_2–C_3 bond in the $^2A_1$ state by 0.05 Å relative to the UHF value but leaves the C_1–C_2 and C_1–C_3 bond lengths unchanged. The structural changes in the $^2B_2$ state are smaller, consisting of a reduction by 0.02 Å in the longer C_1–C_2 and C_1–C_3 bonds and a lengthening by just 0.01 Å in the C_2–C_3 bond. Structure **5a** is still not a minimum at the UMP2 optimized level, although the imaginary frequency has diminished considerably in magnitude ($172i$ cm^{-1}, b_2) relative to its UHF value ($518i$ cm^{-1}), and rearrangement to **4a** occurs also at the UMP2/6-31G* level of geometry optimization without any sign of an energy barrier. The stationary point **5a** ($^2B_2$) may thus be viewed as the transition state for interconversion of equivalent **4a** ($^2A_1$) structures. The small structural changes obtained upon reoptimization at the correlated level lead to only modest changes in the relative energies of the two cyclopropane cation states. Thus, at the CISD level (CISD/6-31G*//UMP2/6-31G* + ΔZPE) the state separation is still 2.2 kcal/mol.[19b] Finally, expansion of the atomic basis sets to 6-311G* (CISD/6-311G*//UMP2/6-31G* + ΔZPE) also gives 2.2 kcal/mol as our best estimate for the energy difference between the two states.[19c] There is no indication from the methods used here that the inverted state order ($^2B_2$ below $^2A_1$) obtained in ref 3 could be correct, nor is there any sign that the $^2A_1$ electronic state in C_{2v} symmetry should not feature a true minimum structure since its lowest vibrational frequency is computed above 500 cm^{-1} at both the UHF/6-31G* and UMP2/6-31G* levels of theory.

The optimized ring geometries of the 2,3-dimethyl species (numbering scheme shown in **4** and **5**), trans (**1d**) or cis (**1e**), are very similar to those calculated for **1a** with only a small lengthening in the C_2–C_3 bond noticeable in both types of radical cation states (Table I). The state ordering computed in **1a** ("$^2A_1$-type" (**4d,e**) below "$^2B_2$-type" (**5d,e**)) is also preserved, but the energetic separation between the two relevant states increases substantially to 8.6 and 8.8 kcal/mol for **1d** and **1e**, respectively (Table II). For the tetramethyl species, **1f**, slightly more pronounced substituent effects are apparent in the values of the optimized structural variables; in particular, the length of the C_2–C_3 bond increases to 1.984 Å (Table I). This feature can be ascribed to steric repulsion across a weak bond; a tendency toward this type of distortion is already apparent for the *cis*-dimethyl derivative, **1e**, which has a C_2–C_3 bond length computed at 1.915 Å compared to 1.888 Å for the *trans*-dimethyl derivative, **1d**. The $^2A_1$–$^2B_2$ energy separation for **1f** exceeds 10 kcal/mol (13.6 kcal/mol; UMP2/6-31G*//UHF/6-31G* + ΔZPE). The equilibrium

(19) (a) $^2A_1$, E(CISD/6-31G*//UHF/6-31G*) = −117.099 50 au; $^2B_2$, E(CISD/6-31G*//UHF/6-31G*) = −117.095 29 au. (b) $^2A_1$, E(CISD/6-31G*//UMP2/6-31G*) = −117.099 89 au; $^2B_2$, E(CISD/6-31G*//UMP2/6-31G*) = −117.095 72 au. (c) $^2A_1$, E(CISD/6-311G*//UMP2/6-31G*) = −117.134 63 au; $^2B_2$, E(CISD/6-311G*//UMP2/6-31G*) = −117.130 40 au.

structures for the "$^2A_1$-type" states are minima in all these species whereas all the stationary points located for the "$^2B_2$-type" states are transition-state structures, each having just one imaginary frequency (**1d**, 505*i* cm^{-1}, b_2 symmetry; **1e**, 509*i* cm^{-1}, a″ symmetry; **1f**, 560*i* cm^{-1}, b_2 symmetry). As in **1a**, the in-plane normal mode corresponding to the imaginary frequency has the proper symmetry to lower the molecular symmetry (**1a,f**, $C_{2v} \rightarrow C_s$; **1d**, $C_2 \rightarrow C_1$; **1e**, $C_s \rightarrow C_1$) and couple the two JT split electronic states (e.g., **1a**, $B_2 \otimes b_2 = A_1$), thus facilitating rearrangements to the "$^2A_1$-type" structures.[7b]

In sharp contrast to all these results, the "$^2B_2$-type" states are favored over the "$^2A_1$-type" states for the 1-methylcyclopropane (**1b**) and 1,1-dimethylcyclopropane (**1c**) cations by 4.7 and 10.3 kcal/mol, respectively. However, the stationary points located for the "$^2A_1$-type" states (**4b,c**) still represent minima on the potential energy surfaces whereas the points of the "$^2B_2$-type" states (**5b,c**), despite now representing the lower energy states, remain transition-state structures with one imaginary frequency of magnitude near 550*i* cm^{-1} (**5b**, 553*i* cm^{-1}, a″ symmetry; **5c**, 564*i* cm^{-1}, b_2 symmetry). The normal mode form (shown for **5b** as **6**) indicates that the total energy will decrease upon in-plane distortion which opens the $C_1C_2C_3$ angle and shortens the C_1–C_2 bond but lengthens the C_1–C_3 bond.

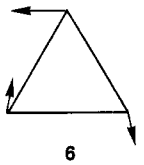

6

Distortion of **5b** or **5c** along this direction and reoptimization leads to a second set of minima on the potential energy surfaces for **1b** and **1c** (**7**; lowest vibrational frequency ~ 190 cm^{-1} in **7b** (^2A), 130 cm^{-1} in **7c** ($^2A'$)). Relative to (transition state) structure

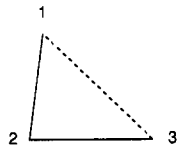

7

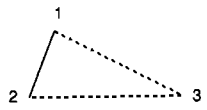

8

5, the $C_1C_2C_3$ angle has in **7** opened up by nearly 20°, the C_1–C_2 bond length has decreased by ~0.20 Å, and the C_1–C_3 and C_2–C_3 bond lengths have increased by ~0.25–0.30 Å and almost 0.10 Å, respectively. Structure **7** may thus be viewed as "$^2A_1$-type" with the methyl substituent on a carbon participating in the one-electron bond; in **4**, the substituent is attached to a conventionally bonded carbon atom. Energetic stabilizations of 5–6 kcal/mol are obtained for **7** relative to **5** at the UHF/6-31G* level but diminished to only 2.1 kcal/mol (**1b**) and 2.6 kcal/mol (**1c**) at the correlated level (MP4, Table II). The energy difference between the two minima represented by **4b** and **7b** is 6.8 kcal/mol in favor of **7b**; the corresponding separation between **4c** and **7c** is 12.9 kcal/mol, showing a near additive effect of the substituent methyl groups.

For both **1b** and **1c**, the symmetrical "$^2B_2$-type" complexes (**5**) may be viewed as transition states for the topomerization between two equivalent minima with nonsymmetric geometries (**7**). There must then be transition states connecting the inequivalent minima, **4** and **7**, on the potential energy surfaces as well. These transition structures (**8**) were located and found to have a substantial in-plane imaginary frequency for both 1-methylated species (**8b**, 590*i* cm^{-1}; **8c**, 584*i* cm^{-1}). For the monomethyl derivative, **8b** (^2A) is computed to be 7.5 kcal/mol above **7b** (^2A) (0.7 kcal/mol above **4b** ($^2A'$)) with the following C–C bond lengths: C_1–C_2 = 1.404 Å, C_2–C_3 = 1.727 Å, and C_1–C_3 = 1.645 Å. The presence of one short but two longer and nearly equal bonds makes **8** resemble a distorted version of the symmetrical (transition state) structure located for the "$^2B_2$-type" states (**5**). For the dimethyl derivative, structure **8c** ($^2A'$) has an even more unsymmetrical structure (C_1–C_2 = 1.417 Å, C_2–C_3 = 1.764 Å, C_1–C_3 = 1.607 Å) and is

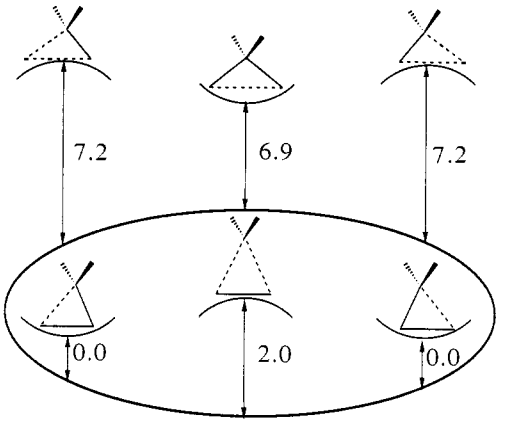

Figure 1. Minima and transition states on the potential energy surface of the radical cationic states of 1-methylcyclopropane (PMP4/6-311G*//UMP2/6-31G* + ΔZPE; relative energies in kcal/mol).

computed to be 12.3 kcal/mol above **7c** ($^2A'$). **8c** is just slightly above **4c** ($^2A_1$) at the UHF level (~1.0 kcal/mol), the computational level used for locating the stationary points, but this difference is virtually nullified after correlation energy has been included and, after ZPE corrections are made, we actually compute **8c** to be below **4c** in energy by 0.6 kcal/mol.

Given the dramatic reduction in the magnitude of the imaginary frequency of **5a** upon the inclusion of correlation (~350*i* cm^{-1}, see above), the appearance of the very long bond in **7b,c** (~1.9 Å), and also the similar energies of transition states **8b,c** and minima **4b,c** (ΔE ~ 0.5 kcal/mol), we deemed it appropriate to examine the radical cationic states of **1b** further at higher computational levels. Geometry optimization at the UMP2/6-31G* level leads mostly to substantial reductions in the large bond lengths with only slight changes occurring in the "normal" bond lengths (Table I). For example, the long C_2–C_3 bond length in **4b** ($^2A'$) is reduced by 0.05 Å, and the C_1–C_3 bond in **7b** (^2A) is shortened by nearly 0.1 Å from 1.91 Å to 1.83 Å. The transition state connecting **4b** and **7b** moves distinctly closer to the "$^2A_1$-type" structure (**4b**) upon reoptimization including correlation. The differences in C–C bond lengths between the two stationary points **4b** and **8b** are now only on the order of 0.05 Å, whereas they are at least twice as large at the UHF level. We have not reevaluated the vibrational frequencies at the correlated level, but at these UMP2/6-31G* optimized geometries the relative energies for the four states of **1b** are as follows: **7b** (0.0, ^2A), **5b** (2.0 kcal/mol, $^2A''$), **4b** (7.0 kcal/mol, $^2A'$), and **8b** (7.3 kcal/mol, ^2A). Thus, they show the same state ordering and basically the same relative energies as obtained previously at the UHF/6-31G* geometries (see above), although the difference between **4b** and **8b** has diminished to only 0.3 kcal/mol. At the expanded basis set (6-311G*) level, the following relative energies are obtained (PMP4(SDTQ)/6-311G*//UMP2/6-31G* + ΔZPE): **7b** (0.0 kcal/mol), **5b** (2.0 kcal/mol), **4b** (6.9 kcal/mol), and **8b** (7.2 kcal/mol); these values are virtually indistinguishable from the values just listed.[20] This supports the idea that, on the correlated potential energy surface, **7b** remains the primary, global minimum and **4b** forms a secondary, local minimum; furthermore, **5b** represents the transition state for interconversion of equivalent **7b** structures, and **8b** is the transition state between structures **7b** and **4b**. The relative energies of these structures are compared in Figure 1.

It thus appears that geometrical distortions and energy barriers predicted on the basis of UHF geometries are exaggerated in cyclopropane radical cations. The potential energy surfaces are flatter at the correlated levels of calculation, but the relative energies computed from correlated wave functions are, overall, rather insensitive to the basis set (6-31G* vs 6-311G*) or the level of theory applied in the geometry optimizations (UHF/6-31G*

(20) The PMP4/6-311G*//UMP2/6-31G* total energies (in au) for **1b** are −156.407 43 (**7b**), −156.404 07 (**5b**), −156.396 33 (**4b**), and −156.395 40 (**8b**).

Table III. Net Charge and Spin Density Distributions for the Cyclopropane Cations **1a-f** (UHF/6-31G*//UHF/6-31G*)

		net positive charge[b]				net spin density			
species[a]	state	C_1	C_2	C_3	C_4	C_1	C_2	C_3	C_4
4a	$^2A_1$	0.248	0.376	0.376		−0.117	0.611	0.611	
5a	$^2B_2$	0.303	0.349	0.349		0.849	0.128	0.128	
4b	$^2A'$	0.083	0.366	0.366	0.184	−0.124	0.611	0.611	0.035
7b	^2A	0.241	0.223	0.323	0.213	0.510	−0.102	0.744	−0.039
4c	$^2A_1$	−0.092	0.362	0.362	0.185	−0.134	0.610	0.610	0.039
7c	$^2A'$	0.120	0.204	0.256	0.210	0.376	−0.107	0.938	−0.036
4d	^2A	0.217	0.199	0.199	0.192	−0.102	0.645	0.645	−0.050
5d	^2B	0.271	0.172	0.172	0.192	0.911	0.113	0.113	0.008
4e	$^2A'$	0.215	0.201	0.201	0.191	−0.103	0.650	0.650	−0.049
5e	$^2A''$	0.270	0.174	0.174	0.191	0.914	0.112	0.112	0.006
4f	$^2A_1$	0.198	0.057	0.057	0.172	−0.092	0.694	0.694	−0.062
5f	$^2B_2$	0.254	0.012	0.012	0.181	0.953	0.112	0.112	0.005

[a] See structures **4**, **5**, **7**, and **8** for numbering scheme; C_4 is the methyl carbon. [b] Charges on hydrogen atoms are summed in with the carbon atoms.

Table IV. Net Charge and Spin Density Distributions for the Cyclopropane Cations **1a** and **1b** at the MP2/6-31G* Optimized Geometries

		net positive charge[b]				net spin density			
species[a]	state	C_1	C_2	C_3	C_4	C_1	C_2	C_3	C_4
				UHF/6-31G*//UMP2/6-31G*					
4a	$^2A_1$	0.253	0.373	0.373		−0.112	0.602	0.602	
5a	$^2B_2$	0.308	0.346	0.346		0.821	0.136	0.136	
4b	$^2A'$	0.096	0.361	0.361	0.183	−0.115	0.602	0.602	0.035
7b	^2A	0.218	0.233	0.344	0.206	0.571	−0.088	0.647	−0.044
				UMP2/6-31G*//UMP2/6-31G*					
4a	$^2A_1$	0.250	0.375	0.375		0.008	0.537	0.537	
5a	$^2B_2$	0.349	0.325	0.325		0.757	0.151	0.151	
4b	$^2A'$	0.107	0.355	0.355	0.182	0.022	0.530	0.530	0.024
7b	^2A	0.214	0.223	0.345	0.219	0.504	0.028	0.554	−0.015
				UMP2/6-311G*//UMP2/6-31G*					
4a	$^2A_1$	0.237	0.382	0.382		0.035	0.535	0.535	
5a	$^2B_2$	0.353	0.324	0.324		0.739	0.161	0.161	
4b	$^2A'$	0.036	0.381	0.381	0.201	0.042	0.528	0.528	0.018
7b	^2A	0.195	0.216	0.359	0.229	0.499	0.060	0.558	−0.010

[a] See structures **4**, **5**, **7**, and **8** for numbering scheme; C_4 is the methyl carbon. [b] Charges on hydrogen atoms are summed in with the carbon atoms.

Table V. Comparison between Calculated and Experimentally Assigned Hyperfine Coupling Constants (G) for Selected Cyclopropane Radical Cations (UHF/6-31G*//UHF/6-31G*)[a]

	$H(C_1)$			$H(C_2)$			$H(C_3)$			$H(C_4)$		
species[b,c]	calcd	exptl	ratio	calcd	exptl	ratio	calcd	exptl	ratio	calcd	exptl	ratio
4a ($^2A_1$)	25.4	21.0	1.21	−23.5	−12.5	1.88	−23.5	−12.5	1.88			
5a ($^2B_2$)	−34.3			5.9			5.9					
4b ($^2A'$)	25.2			−23.7			−23.7			−0.8		
7b (^2A)	−18.8			24.0			−28.2			16.4		
4c ($^2A_1$)				−23.5			−23.5			−1.0		
7c ($^2A'$)				21.9			−34.5			11.4		
4d (^2A)	23.4	21.8	1.07	−23.0	−11.9	1.93	−23.0	−11.9	1.93	18.5	21.8	0.85
4e ($^2A'$)	23.5	20.5	1.14	−22.6	−10.4	2.17	−22.6	−10.4	2.17	16.4	20.5	0.80
4f ($^2A_1$)	23.2	18.7	1.21							13.7	15.0	0.91

[a] Calculated using a = 1600(FCT), where FCT = computed Fermi contact term (in gauss; see text). [b] See structures **4**, **5**, **7**, and **8** for numbering scheme. [c] Electronic state symmetry given in parenthesis. [d] C_4 is the methyl carbon.

or UMP2/6-31G*). All minima on the potential energy surfaces correspond to structures with "$^2A_1$-type" states (**4** or **7**), whereas all "$^2B_2$-type" electronic states produce only transition structures (**5** or **8**).

The hexamethyl-substituted cyclopropane radical cations (C_{2v} symmetry) have also been optimized at the UHF/6-31G* level. The C–C bond lengths in the $^2A_1$ state are C_1–C_2 = C_1–C_3 = 1.507 Å and C_2–C_3 = 1.946 Å, whereas the $^2B_2$ state is structurally characterized by bond lengths of C_1–C_2 = C_1–C_3 = 1.721 Å and C_2–C_3 = 1.427 Å. As expected, the latter structure is a transition state for interconversion of equivalent $^2A_1$ structures. Furthermore, it rearranges spontaneously to the $^2A_1$-state geometry upon in-plane distortion.[21] The barrier to interconversion of equivalent $^2A_1$ states is computed at 4.8 kcal/mol (UHF/6-31G*//UHF/6-31G* + ΔZPE), but inclusion of correlation energy corrections would undoubtedly diminish this value. We have verified above that the **5a**–**4a** ($^2B_2$–$^2A_1$) conversion also proceeds without a barrier in the parent cation, **1a**. These two high-symmetry species possess three equivalent minima (**4**, $^2A_1$) and three equivalent transition states (**5**, $^2B_2$) on the pseudorotation surface. For **1b** and **1c**, the three minima split into two types. Two equivalent absolute minima (**7b,c**) correspond to low-symmetry "$^2A_1$-type" states separated by a small barrier. These minima are substantially below the higher symmetry "$^2A_1$-type" minimum (**4b,c**), which is very shallow. We have not investigated interconversions directly for **1d–f**, but given the considerable energy separation between structures **4** and **5** in these species, we find it unlikely that the alternative "$^2A_1$-type" minima (**7**) can be anything but shallow and close in energy to **5**, i.e., well above **4**.

Net Charge and Spin Density Distributions. Substantial differences in charge and spin distributions exist among the stationary points located for the radical cationic states of **1** (Tables II–V).

(21) The normal mode analysis and the $^2B_2 \rightarrow {}^2A_1$ rearrangement were carried out at the Hartree–Fock level with the split-valence 3-21G basis set only.

The computed values at the UHF level (Table III) fully support the interpretation given above: all minima are of the "$^2A_1$ type" and all transition states are of the "$^2B_2$ type". The justification is most readily made from inspection of the unpaired spin densities. The $^2A_1$ state in **1a** has the unpaired electron distributed on C_2 and C_3 whereas in the $^2B_2$ state it is located largely on C_1. Thus, the unpaired spin is located primarily on the termini of the one-electron bond in all structures of type **4**, whereas all type **5** (and **8**) structures show the unpaired spin largely on the methylenic carbon. In the absolute minima for **1b** and **1c**, structure type **7**, the one-electron bond is between C_1 and C_3. These two atoms carry the unpaired spin density, though it is shared unevenly, particularly in **1c**.

We have also investigated whether the charge and spin density distributions of **1a** and **1b** are significantly altered by moderate changes in geometry or the use of a correlated wave function for the analysis. The effects of geometry changes are illustrated by comparison of the UHF values computed at the optimized UMP2 geometries (Table IV, top) with those computed at the UHF geometries (Table III). As expected, differences between the two sets of data are generally small but grow in magnitude when certain aspects of the UHF and UMP2 geometries differ to a larger extent. For example, in structure **7b** the C_1–C_3 one-electron bond length was shortened by almost 0.1 Å at the correlated level, and this is reflected in a more even spin density distribution between these two atoms at the UMP2 geometry. The population analysis using the one-electron reduced density matrix from the UMP2 wave function (Table IV, middle) does not change the densities dramatically relative to the UHF values (Table IV, top), but a general smoothing of values does appear to take place. Thus, with the correlated wave function the maximum unpaired spin density values are diminished and the small negative spin densities occasionally computed at the UHF level on a central ring atom are no longer present. Finally, expansion of the basis set to 6-311G* (Table IV, bottom) from 6-31G* has only small effects on the computed spin and charge distributions.

The Fermi contact terms, also computed at the UHF level, are the basis for the ^1H hyperfine coupling constants shown in Table V. The calculated hyperfine coupling constants are of particular interest. These parameters can be derived directly from the ESR spectra of the cyclopropane radical cation and several methyl-substituted derivatives, and they form the basis on which the structures of **4a**, **4d**, **4e**, and **4f** were assigned.[10] A comparison between calculated and experimental results (Table V) should be illuminating.

^1H hyperfine coupling constants (hfc's) are related to the carbon spin densities at adjacent carbon centers by different mechanisms of interaction. For π radicals, there are two principal mechanisms, involving either an exchange interaction or hyperconjugation. Protons attached directly to carbon atoms bearing positive spin density have negative hfc's because of the preferred exchange interaction between the unpaired π spin density and the carbon σ electrons (π,σ polarization). On the other hand, ^1H nuclei which are one C–C bond removed from a carbon bearing positive spin density usually interact by hyperconjugation. This mechanism causes the π spin density on carbon to be delocalized onto ^1H nuclei, resulting in a positive hyperfine coupling constant.

The comparison between experiment and theory shows poor agreement only for the negative hyperfine coupling constants: the ratio of calculated to experimental values for the hfc's of **4a**, **4d**, and **4e** ranges from 1.88 to 2.17. Clearly, the ab initio calculations significantly overestimate the coupling constants resulting from π,σ polarization, even when the structures are optimized at the UHF/6-31G*//UHF/6-31G* level. In contrast, positive coupling constants caused by hyperconjugative interaction between protons and the unpaired spin are generally reproduced quite well. The coupling of rigid ^1H nuclei is calculated consistently high (**4a,d–f**; calcd/exptl = 1.07–1.21), whereas the coupling of methyl protons is calculated consistently low (**4d–f**; calcd/exptl = 0.80–0.91).

Other systems, for which calculated and experimental hyperfine couplings are available, also show poor agreement for the negative splittings caused by π,σ polarization, whereas the positive splittings due to hyperconjugation are, once again, reproduced fairly well. For example, the olefinic protons of norbornadiene radical cation are overestimated significantly (UHF/6-31G*; calcd[22]/exptl[23] = 1.67), whereas the bridge protons two C–C bonds removed from the unpaired spin (coupled by "homo" hyperconjugation) are calculated considerably better (calcd/exptl = 0.92).[22,23] Interestingly, the small negative bridgehead (β) coupling, documented by both CIDNP[24] and ESR/ENDOR results,[23] is reproduced reasonably well (calcd/exptl = 1.4).[22] This coupling was ascribed to "residual" π,σ polarization,[23] an interaction usually obscured by the much stronger hyperconjugative interaction. For the norbornadiene radical cation, however, hyperconjugation is inefficient, because the bridgehead protons lie in the nodal plane of the SOMO.[23]

Results obtained for the bicyclobutane radical cation show similar trends. For this system, the bridgehead carbons bear positive spin density, documented by both CIDNP[25] and ESR/ENDOR results;[26] the hyperfine coupling constants of the corresponding protons are overestimated significantly[27] (UMP2/6-31G*; calcd/exptl = 2.38), whereas the geminal protons in the exo and particularly the endo positions are calculated considerably better (endo, calcd/exptl = 0.997; exo, calcd/exptl = 1.21).[27]

The ab initio calculations may actually reproduce some of the positive hfc's even more closely than the comparison with experimentally assigned values suggests. The disagreements noted between calculated and assigned hfc's may be due, in part, to inaccuracies in the experimentally derived values. The ESR spectra of **4a,d–f** were obtained in frozen matrices; the line widths typical for these conditions (≥3 G) introduce some latitude in the simulation of the spectra and, correspondingly, in the assigned hfc's. To probe this assertion, we have simulated the reported ESR spectra[10] of **4d** and **4e** using our calculated hfc's for $H(C_{1,3})$ (23.5 G instead of 21.5 G) along with the values for $H(C_2)$ and $H(C_4)$ derived by Williams and co-workers. These simulations are in satisfactory agreement with the experimental spectra; the spectral patterns of line positions, intensities, and widths are reproduced as well as or better than those produced with the data chosen by Williams and co-workers.

Of the cyclopropane radical cations discussed here, the structure (**7c**) calculated for the 1,1-dimethyl derivative appears particularly interesting. The predicted unsymmetrical minimum has three distinct sets of hyperfine couplings; of these, one is unexceptional ($H(C_2)$ hfc = 21.9 G), whereas the other two are significantly different from those of any previously reported cyclopropane radical cation. The predicted coupling for the protons of the geminal methyl groups (11.4 G) is lower than any methyl coupling found for a cyclopropane system: the hfc's calculated for the methyl protons of **4d–f** range from 18.5 to 13.7 G, compared to assigned values ranging from 21.8 to 15.0 G. In contrast, the predicted coupling of the methylene protons at C_3 (−34.5 G) is significantly higher than any hfc calculated for the corresponding protons of **4a–e** (−22.6 to −23.7 G). Although this coupling is likely to be substantially overestimated, its actual value should still be significantly higher than those assigned to **4a,d,e** (−12.5 to −10.4 G).[10] The diminished coupling for the methyl protons of **7c** is in line with the diminished spin density at C_1 (**7c**, ρ_1 = 0.38; **4f**, $\rho_{2,3}$ = 0.69), whereas the high coupling constant predicted for $H(C_3)$ is in line with the high spin density at this secondary carbon (ρ_3 = 0.94). This value is considerably higher than that predicted for any secondary (**4a–c**, $\rho_{2,3}$ = 0.61), tertiary (**4d,e**, $\rho_{2,3}$ = 0.65), or quaternary carbon (**4f**, $\rho_{2,3}$ = 0.69).

The trend to an unsymmetrical spin density distribution, with lower spin density at the substituted ring carbon (C_1) and higher

(22) Raghavachari, K.; Haddon, R. C.; Roth, H. D. *J. Am. Chem. Soc.* **1983**, *105*, 3110–3115.
(23) Gerson, F.; Qin, X.-Z. *Helv. Chim. Acta* **1989**, *72*, 383–385.
(24) Roth, H. D.; Schilling, M. L. M.; Jones, G., Jr. *J. Am. Chem. Soc.* **1981**, *103*, 1246–1248.
(25) Roth, H. D.; Abelt, C. J.; Schilling, M. L. M. *J. Am. Chem. Soc.* **1985**, *107*, 4148–4152.
(26) Gerson, F.; Qin, X.-Z.; Ess, C.; Kloster-Jensen, E. *J. Am. Chem. Soc.* **1989**, *111*, 6456–6457.
(27) Roth, H. D.; Lakkaraju, P. Unpublished results.

spin density at C_3, and correspondingly divergent hfc's for $H(C_1)$ and $H(C_3)$, is foreshadowed in the preferred structure (**7b**) calculated for the monomethyl derivative ($\rho_1 = 0.51$, hfc = −18.8 G; $\rho_3 = 0.74$, hfc = −28.2 G). Clearly, **7b** and **7c** are unusual and unprecedented cyclopropane radical cations; their structures merit experimental verification. Appropriate experiments for the dimethyl derivative are under way.

Concluding Remarks

We conclude that even simple alkyl substituents are capable of significantly altering the shapes of the potential energy surfaces of cyclopropane radical cations, always preferentially stabilizing the "$^2A_1$-type" states possessing a long, one-electron C–C bond.[28] Localization of the UHF/6-31G* wave function using the natural bond orbital analysis procedures developed by Weinhold et al.[29] progresses smoothly; in **4a**, for example, this procedure predicts that a C_2–C_3 bond orbital containing 0.97 electron is formed almost exclusively (>95%) by C(2p) atomic orbitals. Despite the bonding characteristics exemplified by cyclopropane orbital **3**, all "$^2B_2$-type" states are low-energy transition states for interconversion of equivalent "$^2A_1$-type" minima. The predicted fine-tuning of the preferred geometry and resulting charge and spin distributions for substituted cyclopropane cations should be qualitatively verifiable by a combination of chemical (e.g., nucleophilic substitution) and spectroscopic (principally ESR and CIDNP) experiments. Such experiments are under way in our laboratories.

Acknowledgment. The computational work was made possible by equipment grants from the National Science Foundation, the National Institutes of Health, and the New Jersey Commission on Science and Technology.

Supplementary Material Available: The optimized geometries of all stationary points for species **4**, **5**, **7**, and **8** in **Z**-matrix format (20 pages). Ordering information is given on any current masthead page.

(28) A referee has questioned whether diffuse functions should have been added to the basis set to properly describe this long C–C bond. We have used the 6-31G* basis set throughout our geometry optimizations. This basis set is of split-valence quality on all the atoms and contains d-type polarization functions on the carbon atoms as well. In **4a** at the UHF/6-31G* level, we obtained C_1–C_2 and C_2–C_3 bond lengths of 1.477 and 1.875 Å, respectively (Table I). Addition of diffuse valence functions to the basis set on the carbon atoms only (6-31G* → 6-31+G*) and reoptimization leads to equilibrium C_1–C_2 and C_2–C_3 bond lengths of 1.477 and 1.877 Å, respectively. These values are unchanged upon addition of diffuse functions to the hydrogen atoms (6-31+G* → 6-31++G*). Addition of p-type polarization functions on the hydrogen atoms (6-31++G* → 6-31++G**) and reoptimization gives C_1–C_2 and C_2–C_3 bond lengths of 1.476 and 1.876 Å, respectively, for **4a**. We conclude that the 6-31G* basis set is adequate for the description of the structural features of cyclopropane cations and that the role played by diffuse basis functions is minimal.

(29) Carpenter, J. E.; Weinhold, F. *J. Mol. Struct.: THEOCHEM* **1988**, *169*, 41–62. Foster, J. P.; Weinhold, F. *J. Am. Chem. Soc.* **1980**, *102*, 7211.

Reaction of Alkynes with Cyclopropylcarbene–Chromium Complexes: A Versatile [4 + 2 + 1 − 2] Cycloaddition Reaction for the Construction of Cyclopentenones

Seniz U. Tumer, James W. Herndon,* and Leonard A. McMullen

Contribution from the Department of Chemistry and Biochemistry, University of Maryland, College Park, Maryland 20742-2021. *Received December 27, 1991*

Abstract: The scope and limitations of the reaction between cyclopropylcarbene–chromium complexes and alkynes have been examined. A variety of cyclopropylcarbene complexes and alkynes have been employed in these studies. The reaction appears to be general for most simple alkynes, producing cyclopentenones. A mechanism has been proposed involving metallacyclobutene formation, electrocyclic ring opening, electrocyclic ring closure, CO insertion, alkene insertion, metallacyclopentene fragmentation, and cyclopentadienone reduction. The presence of these intermediates has been inferred from the structure of products obtained when the reaction was conducted in acetonitrile instead of dioxane. A trapping experiment employing 1,6-heptadiyne supports the intermediacy of vinylcarbene or vinylketene complexes.

Introduction

The reaction between alkynes and α,β-unsaturated carbene–chromium complexes, which produces aromatic rings[1] in addition to other types of products, has emerged as a powerful tool for the synthetic organic chemist. A diverse array of natural products has been synthesized using this reaction, including anthraquinone anticancer agents,[2] naphthoquinone antibiotics,[3] vitamin E,[4] khellin,[5] and psoralen derivatives.[6] In all of these reactions, a carbene complex containing an unsaturated substituent at the carbene carbon (e.g., complex **2**) was employed, and the unsaturated substituent and the carbene carbon were later incorporated into the newly-formed aromatic ring system. As part of a program to develop a general cycloaddition reaction for the synthesis of carbocyclic seven-membered rings, we have examined the reaction

Scheme I. Reaction of Alkynes with α,β-Unsaturated Carbene Complexes and Cyclopropylcarbene Complexes

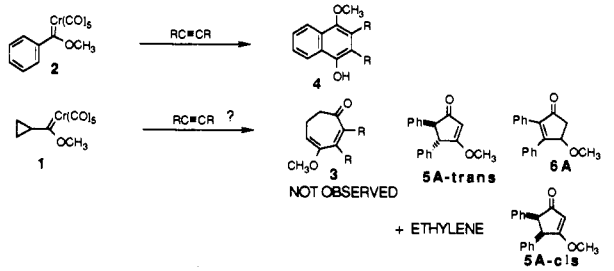

(1) (a) For a review of metal–carbene complexes, see: Doetz, K. H. *Angew. Chem., Int. Ed. Engl.* **1984**, *23*, 587–608. (b) Wulff, W. D. In *Advances in Metal-Organic Chemistry*; Liebeskind, L. S., Ed.; JAI Press: Greenwich, CT, 1989; Vol. 1.

(2) Wulff, W. D.; Xu, Y.-C. *J. Am. Chem. Soc.* **1988**, *110*, 2312–2314.

(3) Semmelhack, M. F.; Zask, A. *J. Am. Chem. Soc.* **1983**, *105*, 2034–2043.

(4) Doetz, K. H.; Kuhn, W. *Angew. Chem. Int. Ed. Engl.* **1983**, *22*, 732.

(5) Yamashita, A.; Toy, A.; Scahill, T. A. *J. Org. Chem.* **1989**, *54*, 3625–3634.

(6) Wulff, W. D.; McCallum, J. S.; Kunng, F.-A. *J. Am. Chem. Soc.* **1988**, *110*, 7419–7434.

0002-7863/92/1514-8394$03.00/0